THE JOURNAL OF PHYSICAL CHEMISTRY C
A JOURNAL OF THE AMERICAN CHEMICAL SOCIETY

pubs.acs.org/JPCC
Article

Open Metal Sites Govern Hydration Kinetics and Molecular Fluctuations in Metal−Organic Frameworks

Arda Yildirim, Paulina Szymoniak, Tabea C. V. Haug, Michael Fröba,* Patrick Huber,* and Andreas Schönhals*

Cite This: https://doi.org/10.1021/acs.jpcc.6c02160
Read Online

ABSTRACT: Water under nanoscale confinement exhibits structural and dynamical states distinct from bulk behavior, yet the role of pore chemistry in governing these states remains insufficiently understood. Herein, the hydration kinetics and molecular-scale fluctuations of water confined within a comprehensive series of MOF-74 metal-organic frameworks incorporating Mg, Ni, Co, and mixed-metal compositions were investigated and compared with those observed in mesoporous MCM-41 silica. In situ impedance spectroscopy resolves a pronounced multistep hydration mechanism in MOF-74, initiated by rapid coordinative binding at open metal sites, followed by cluster formation and final capillary condensation. In contrast to MCM-41 silica, where capillary condensation dominates, the presence of coordinatively unsaturated metal centers fundamentally alters adsorption pathways. Mixed-metal MOF-74 exhibits accelerated and temporally broadened hydration, reflecting heterogeneous distributions of adsorption energies. Broadband dielectric spectroscopy reveals a distinct water-specific relaxation process (w-relaxation) attributed to fluctuations of water clusters interacting with metal nodes. Relaxation rates follow Arrhenius behavior with activation energies increasing in the order Mg < Ni < Co and further enhanced in mixed-metal systems. Remarkably, water confined within MOF-74 remains liquid-like down to 133 K without crystallization, whereas crystallization is observed in MCM-41 silica. All activation data of the MOF-74 systems obey a common Meyer−Neldel compensation relation, indicating cooperative molecular dynamics and suggesting a hindered glass-transition−like process of confined water clusters. These findings demonstrate that open metal sites and metal composition enable programmable control over hydration kinetics and collective water dynamics in microporous frameworks. MOF-74 thus provides a tunable model platform for engineering water-driven transport, catalysis, and energy-relevant processes at the nanoscale.

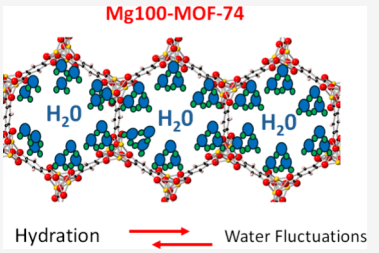

INTRODUCTION

Water is universally recognized as the most critical liquid for sustaining life, serving as an indispensable component for biological and ecological systems.[1] Despite its fundamental role, water remains a subject of extensive scientific research due to its numerous anomalies and atypical physicochemical properties. The underlying molecular mechanisms of these properties are not yet fully understood.[2] Although liquid bulk water represents the most familiar state, water frequently occurs in spatially confined environments, as observed in numerous biochemical[3−8] and geochemical processes.[9−12] A spatial confinement can significantly alter the structural and dynamic properties of water compared to the bulk phase, making it a subject of considerable scientific interest.[13] The most important confinement effect on water is that the freezing point is lowered,[14] allowing water to stay in a liquid nonfreezable state (supercooled liquid) at subzero temperatures.[15,16] This nonfreezable water can even undergo a glass transition, which means a thermo-kinetic transition from the supercooled liquid to an amorphous solid state. Investigations on confined water can further help to understand the behavior of bulk water in the temperature range, which is called the no-man's temperature range (150−235 K).[17] An understanding of confined water in an applicational context is necessary for the development of new materials, for instance, that enable effective ion transport, water-driven mechanical actuation, or for water purification, electrical energy storage and conversion, as well as catalysis in a sustainable way, besides others (see, for instance refs 18−22).

Several porous systems have been employed as host systems to confine water. These host systems include silica-based materials like Mobil Compositions of Matter (MCM)[23−33] or SBA-type.[23,34−36] Besides these materials, water was also confined to the pores of anodic aluminum oxide,[37] silicon,[22,38] molecular sieves,[39−43] graphene or graphite oxide.[44] Recently, water was investigated confined to periodic mesoporous organosilicas (PMOs), a special class of metal-free hybrid

Received: April 3, 2026
Revised: June 5, 2026
Accepted: June 23, 2026

materials.[45−55] The structure and molecular mobility of water embedded within the pores of metal−organic frameworks (MOFs) were also investigated.[18,56,57]

MOFs are a relatively new class of porous materials.[58] They are characterized by extremely high Brunauer−Emmett−Teller (BET) surface areas (up to 7800 m^2/g), including a high porosity up to 80%.[58−60] MOFs are organic−inorganic hybrid materials that are built from metal ions or metal ion clusters, referred to as secondary building units (SBUs), which are interconnected by organic linkers. This assembly results in an ordered, crystalline three-dimensional network characterized by well-defined pores, cavities, and channels. By varying the choice of SBUs through the incorporation of different metal ion centers and modifying the organic linkers, an extensive range of structural and chemical diversity can be achieved, with a wide range of pore sizes and shapes.[61−64] Such tunability enables the rational design of MOFs with tailored properties and functionalities optimized for specific applications. Among these applications are gas storage (see, for instance, refs 65−68), water harvesting,[69−71] and drug delivery,[72−74] besides others.

Certain MOFs feature open metal sites (OMS), also referred to as coordinatively unsaturated sites (CUS), within their structure. These sites arise when not all potential coordination positions of the metal centers are occupied by organic linkers. However, during synthesis, these vacant sites are typically coordinated by solvent molecules. Following the synthesis, the activation of MOFs is typically achieved through the removal of residual solvent molecules from the pores and, if present, those coordinated to the metal centers. This process generally involves the application of heat and/or vacuum, and in some cases, prior solvent exchange with a lower-boiling-point solvent to facilitate complete removal. Activation exposes the OMS, which serves as a strong adsorption center for a wide range of molecules, including water.

Here, we study the hydration kinetics and molecular fluctuations of water confined in monometallic and mixed-metal MOF-74 (CPO-27) frameworks.[75] MOF-74 is distinguished by an exceptionally high concentration of coordinatively unsaturated metal sites, making it an ideal platform for investigating water−surface interactions under nanoscale confinement. They are characterized by a framework comprising one-dimensional channels, forming a honeycomb-like architecture. At this point, an important question concerns the spatial distribution of metal ions within mixed-metal MOF-74. Specifically, it remains unclear whether different metal species are incorporated within the same SBU or metal node, or whether each node contains only a single metal species, with the different metals distributed among distinct nodes throughout the framework. There is some experimental evidence that for mixed-metal MOFs, each specific metal node contains only one kind of metal ion and not a mixed-metal center.[76,77] So the framework consists of single metal nodes, but the overall structure of mixed-metal MOF-74 is formed by a mixture of these nodes having different metal ions. However, there is no long-range ordering of the metal nodes, which causes a random distribution of different adsorption sites. It is worth noting that the distribution of the nodes with the different metal ions can be controlled during the synthesis, for instance, by the choice of the solvent.[77]

In the first part of this study, the sorption kinetics of water (hydration) in MOF-74 were studied by an in situ dielectric approach. The interaction of water with some of the considered MOF-74 materials was investigated by FTIR spectroscopy.[57] The results obtained for the different MOF-74 materials were compared to those for MCM-41 silica, which exhibits a similarly ordered hexagonal array of cylindrical pores but lacks specific water adsorption sites beyond those provided by hydrogen-bonding interactions. In contrast, MOF-74 structures possess OMS that enable coordinative bonding of water molecules to the framework. In the second part of this investigation, the molecular fluctuations of water inside the pores are studied by broadband dielectric spectroscopy. The dielectric behavior of the considered MOF-74 materials in the dry state was studied elsewhere.[80]

EXPERIMENTAL SECTION

Materials

Nine different MOF-74 materials having Mg, Ni, and/or Co ions as SBUs were synthesized. For the mixed-metal MOF-74, different ratios of Mg/Co and Mg/Ni have been employed. As a linker, 2,5-dihydroxyterephtalic acid was used. The synthesis was carried out as given in refs 78,79. The synthesized MOF-74 materials have been characterized previously with respect to their metal composition, pore size distribution, pore volume, and BET surface area.[57,80] The characterization also includes XRD measurements. It is worth mentioning that the considered MOF-74 materials contain hydrophilic sites at the metal centers, as well as hydrophobic parts at the phenylene units. For comparison, an MCM-41 silica sample with native hydrophilic pore walls was also investigated. Notably, the pore size of the MCM-41 silica (3.5 nm) is larger than that of the MOF-74 materials (1−1.3 nm). However, both classes of materials have one-dimensional pores arranged on a hexagonal lattice. Details of the composition of MgxNi$(1-x)$-MOF-74 and MgxCo$(1-x)$-MOF-74, pore sizes, and BET surface areas are given in Table 1.

Table 1. Properties of the MOF-74 samples as given elsewhere[80]

sample name	metal composition [mol %]	maximum pore size distribution [nm]	surface area [m^2/g]
Mg100-MOF-74	100% Mg	1.3	1420
Co100-MOF-74	100% Co	1.2	1013
Ni100-MOF-74	100% Ni	1.1	1471
Mg70Co30-MOF-74	70% Mg, 30% Co	1.2	1166
Mg50Co50-MOF-74	50% Mg, 50% Co	1.2	1200
Mg25Co75-MOF-74	25% Mg, 75% Co	1.0	1091
Mg70Ni30-MOF-74	70% Mg, 30% Ni	1.2	1305
Mg50Ni50-MOF-74	50% Mg, 50% Ni	1.2	1243
Mg25Ni75-MOF-74	25% Mg, 75% Ni	1.2	1223
MCM-41 silica		3.5	

Sample Preparation. Water was confined in the cleaned pores of the considered MOF-74 materials with activated OMS. The cleaning and activation procedure for MOF-74 was previously developed and given in ref 80. In brief, after solvent exchange, the pores were cleaned and activated by outgassing the MOF-74 under a vacuum of 10^{-4} mbar at 423 K for 300 min.

Following the cleaning and activation procedures, the samples were transferred under a vacuum into a humidity-controlled glovebox. Subsequently, they were positioned within a custom-designed humidity chamber equipped with an in situ impedance measurement system. A photo of the custom-made sample preparation and the in

https://doi.org/10.1021/acs.jpcc.6c02160
J. Phys. Chem. C XXXX, XXX, XXX−XXX

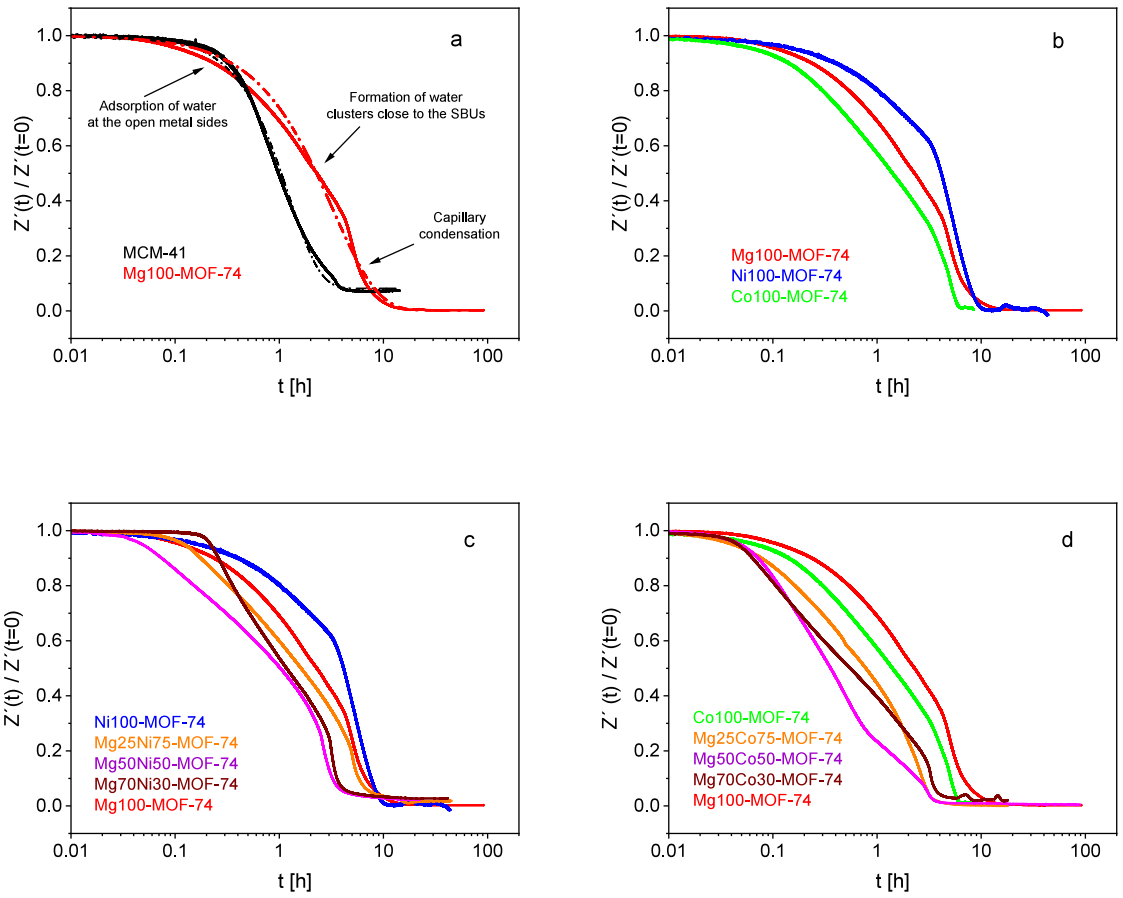

Figure 1. (a) Normalized impedance versus time at a frequency of 1000 Hz for MCM-41 silica (black line) and Mg100-MOF-74 (red line). The dotted-dashed lines represent fits of eq 1b to the corresponding data. (b) Normalized impedance versus time at a frequency of 1000 Hz for the different single-metal MOF-74 materials: red line—Mg100-MOF-74, blue line—Ni100-MOF-74, and green line—Co100-MOF-74. (c) Normalized impedance versus time for the MgxNi(1 − *x*)-MOF-74 as indicated. (d) Normalized impedance versus time for the MgxCo(1 − *x*)-MOF-74 as indicated.

situ impedance measurement setup is given in the Supporting Information in Figure S1. In the chamber, a relative humidity in the range from 5 to 95% can be precisely employed and controlled. The humidity in the chamber was adjusted by bubbling dry nitrogen through a water-containing bottle by controlling the flow rates of nitrogen and the hydrated nitrogen vapor independently.

Moreover, an in situ impedance measurement setup consisting of an LCR meter, LCR-6000 Precision (GW Instek), with a custom-made Teflon sample holder having parallel brass electrodes has been included. The impedance measurement setup allows one to follow the adsorption of water into the pores as a function of time by measuring the real part of the complex impedance $Z'(t)$.

The samples were subjected to a continuous nitrogen−water vapor atmosphere within the controlled chamber, maintaining a relative humidity of 80%. The selected value of humidity is above the value for capillary condensation. This condition was sustained for several hours to facilitate capillary condensation of water within the pores of the MOF-74 structures, ensuring complete pore filling. The temperature at the loading was kept constant at 21 °C due to air conditioning. The pore filling process was quantitatively assessed through real-time impedance monitoring, employing in situ impedance spectroscopy throughout the hydration process as described above.

Dielectric Spectroscopy. The complex dielectric permittivity or function, given by $\varepsilon^*(f) = \varepsilon'(f) - i\varepsilon''(f)$, of the MOF-74 materials containing confined water was measured over a frequency range from 10^{-1} to 10^6 Hz and temperatures from 133 to 293 K using a high-resolution ALPHA analyzer (Novocontrol Technologies, Montabaur, Germany) and the corresponding software. The ALPHA analyzer was interfaced to a sample holder with an active head. Here ε' and ε'' denote the real and imaginary (dielectric loss) parts of the complex dielectric function $\varepsilon^*(f)$. **f** represents the frequency and $i = \sqrt{-1}$ is the imaginary unit. Details of the technique can be found elsewhere.[81] The temperature of the sample was controlled by a Quatro cryostat system (Novocontrol) working with nitrogen as a heating/cooling agent. The stability of the temperature was better than 0.1 K.

For the dielectric measurements, the hydrated samples were filled into a custom-made hermetically sealed cell directly in the controlled humidity chamber. The design of the cell is given elsewhere.[82] By using this cell, the desorption of water during the dielectric measurement was avoided. The measurement was carried out in a parallel plate geometry.

Furthermore, it is important to note that the measurements are carried out on powders. Therefore, the measured samples consist of MOF particles and interparticle spaces filled with air. For this reason, the absolute values of the measured dielectric function is only an observed quantity, and their absolute value is not necessarily correct. However, the position of the maximal dielectric loss is not mainly affected by this factor.

RESULTS AND DISCUSSION

Water Sorption Kinetics

The interaction and adsorption of water are controlled by the interplay of hydrophilic and hydrophobic parts of the framework.[83] The interaction of water with the MOFs was, for instance, studied by infrared spectroscopy, analyzing the OH stretching vibration quantitatively in the literature.[57,84−91]

https://doi.org/10.1021/acs.jpcc.6c02160
J. Phys. Chem. C XXXX, XXX, XXX−XXX

The fitting of three Gaussians was found to be sufficient to describe the OH stretching vibration of the confined water. This approach was also employed for the Mg100-MOF-74, Ni100-MOF-74, and some members of the MgxNi(1 − x)-MOF-74 series.[57] The Gaussian with the lowest wavenumber at ca. 3200 cm^{-1} was assigned to water molecules with a water/water coordination number around 4 with a tetrahedral structure. Such a structure can also be found in ice. Considering that this type of water is most likely the most ordered one, it can be assigned to water molecules forming clusters around the water coordinated at the OMS. Inside these clusters, the water molecules have strong hydrogen bonds. The second mode of the OH stretching vibration observed at 3400 cm^{-1} is attributed to a type of water molecule that is less ordered than that in water clusters. It can be considered confined liquid-like water. In turn, this means that the properties of the confined liquid water are no longer strongly dominated by its interaction with the SBUs for this kind of confined water. Most likely, it forms larger domains or aggregates in the vicinity of the SBUs. The third mode of the OH stretching vibration is located at a wavenumber of 3600 cm^{-1}. It is commonly attributed to single water molecules or multimers of water floating in the center of the pores. It remains unclear whether such multimeric water species can exist in pores that are completely filled. It is worth noting that X-ray scattering combined with thermogravimetric analysis (TGA) also reveals three different states of water for a variety of MOF-74 materials with different metal ions.[92]

The different states of water, as evidenced, for instance, by FTIR measurements, should also be reflected in the adsorption kinetics. Conventionally, the hydration of porous materials is followed by thermogravimetry and/or measuring the adsorbed volume versus pressure, which confirms for MOF systems three different states of water.[92] Here, a different approach is employed by studying the adsorption versus time by a dielectric approach. This approach is possible because water is a polar molecule, and therefore, the whole system becomes more polar when water is absorbed. Figure 1a compares the normalized impedance versus time for MCM-41 silica and Mg100-MOF-74. For both materials, the impedance decreases with time as the adsorbed water molecules are more polar compared to the host materials. As more water is absorbed, the impedance decreases because the entire system becomes more polar.[93] This statement remains correct for the case when the water molecules form an interconnected hydrogen-bonded network, where dipole moments can also be averaged out in a few cases. If the adsorption process is completed, no water is further absorbed, and the impedance becomes a constant value independent of time. This means that by measuring the impedance during pore filling, the kinetics of the pore filling process can be accessed. It is worth noting that besides water adsorption in the pores, water can also be adsorbed at the surface of the grains. However, the BET surface area due to the pores is much larger than the surface area of the grains. Therefore, water adsorption at the surfaces of the grains can be neglected in the adsorption kinetics.

From Figure 1a, several further conclusions can be drawn. To reach a complete pore filling for Mg100-MOF-74, a relatively long time of approximately 20 h is needed, whereas for MCM-41 silica, the time for pore filling is shorter (ca. 5 h). Assuming that the pore size is the dominating factor for adsorption, one might argue that the different time dependences of the adsorption kinetics of the MCM-41 silica and the Mg100-MOF-74 are due to the different pore sizes of both materials. For the case that the pore size is the dominating factor and that the adsorption is diffusion controlled, the time dependence of the adsorption curves should collapse into one chart when the impedance $Z'(t)$ is plotted versus the reduced time $t/(\text{pore size})$. Figure S2 in the Supporting Information depicts $Z'/Z'(t = 0)$ versus t/(pore size) for MCM-41 silica and Mg100-MOF-74. The two data sets do not superimpose in this reduced representation. Therefore, one must conclude that the adsorption process is not diffusion-controlled and that factors such as pore chemistry have a larger influence on the adsorption kinetics than pore size. For MCM-41 silica, the adsorption kinetics show almost one relatively sharp decay in the impedance. Besides hydrogen bonding at the silanol groups at the pore walls, MCM-41 silica has no further specific adsorption sites for water. Therefore, the adsorption of water is most likely due only to capillary condensation.

Further, Figure 1a reveals that the adsorption kinetics of water in the pores of Mg100-MOF-74 are different from those in MCM-41 silica. For Mg100-MOF-74, the time dependence of the normalized impedance shows at least a two-step decay. As discussed above, MOF-74 materials have specific adsorption sites for water at the OMS of the SBUs. At the OMS, water molecules are coordinatively bonded. Compared to hydrogen bonds between water and the silanol groups of the MCM-41 silica, the coordinative bonds of water molecules at the OMS are stronger.[94−96] Therefore, the initial decay of the impedance at short times (for Mg100-MOF-74 up to ca. 0.3 h) is assigned to water molecules forming coordinative bonds with the OMS. For longer times up to ca. 4 h for Mg100-MOF-74, the adsorption kinetics of water is assigned to the formation of water clusters close to the coordinatively bonded water molecules. Finally, the water adsorption at the longest times up to 17 h for Mg100-MOF-74 is assigned to complete pore filling due to capillary condensation.

To discuss the differences in the adsorption kinetics of MCM-41 and Mg100-MOF-74, some modeling has been carried out. Empirically, the adsorption kinetics in porous media have been modeled by the so-called Avrami equation,[97] which reads

$$\frac{M(t)}{M_\infty} = 1 - \exp\left(-\left(\frac{t}{\tau_s}\right)^n\right) \tag{1a}$$

Here $M(t)$ is the adsorbed mass at time t, M_∞ the adsorbed mass for $t\rightarrow\infty$, and τ_s a time constant for the sorption process. In principle, n is a fitting parameter but also carries information about the sorption process. For $n = 0.5$, the process is diffusion-controlled, whereas for $n \geq 1$ the sorption process is more complex. For the impedance, eq 1a can be rewritten as

$$\frac{Z'(t)}{Z'(t=0)} = (1 - Z'^{,\text{red}}_\infty)\exp\left(-\left(\frac{t}{\tau_s}\right)^n\right) + Z'^{,\text{red}}_\infty \tag{1b}$$

Where $Z'^{,\text{red}}_\infty$ is the reduced impedance for $t\rightarrow\infty$. It is worth noting that eq 1 does not include a term that accounts for a special interaction of water with materials like hydrogen bonding or coordinative bonding.

Figure 1a shows the fit of eq 1b to the sorption kinetics of the MCM-41 silica. The data for MCM-41 silica can be reasonably well described by eq 1b, besides some small deviations in the time range between 0.1 and 1 h (see Figure S3, plot of the relative residuals). These deviations might be

https://doi.org/10.1021/acs.jpcc.6c02160
J. Phys. Chem. C XXXX, XXX, XXX−XXX

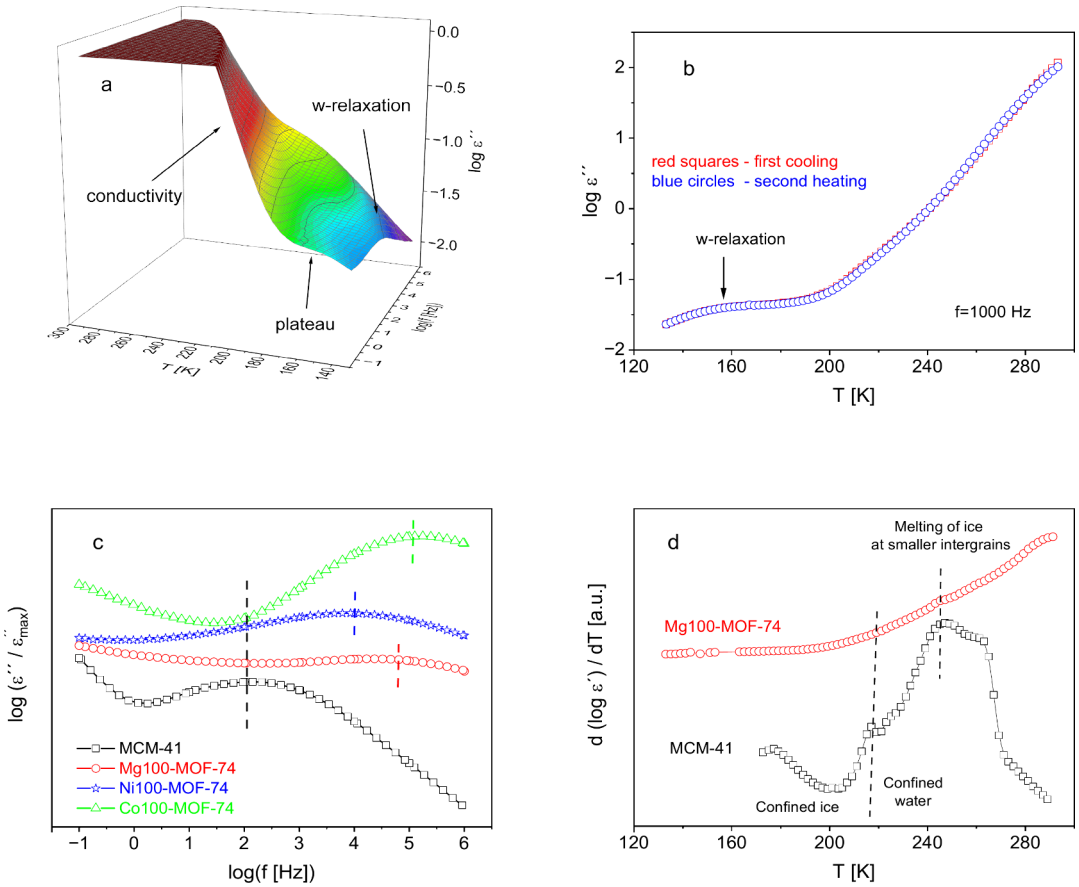

Figure 2. (a) Dielectric loss versus frequency and temperature for Mg100-MOF-74 in a 3D representation. (b) Dielectric loss versus temperature at a frequency of 1000 Hz: Comparison of the first cooling and the second heating run. (c) Dielectric loss normalized by the maximum dielectric loss of the w-relaxation process versus frequency at a temperature of 173 K (−100 °C) for the single-metal MOF-74 materials and the MCM-41 silica as indicated. The curves were shifted along the y-scale for clarity. (d) Derivative d (log ε'')/dT versus temperature at a frequency of 1000 Hz: red circles—Mg100-MOF-74 and black squares—MCM-41 silica. The curves were shifted along the y-scale for clarity.

due to hydrogen bonding between water molecules and the silanol groups of MCM-41 silica. Moreover, the parameter n is found to be 1.45, indicating that the sorption behavior is not diffusive.

The fit of eq 1b to the data of Mg100-MOF-74 is included in Figure 1a. The sorption kinetics of Mg100-MOF-74 are not well described by eq 1b. This becomes obvious from the plot of the relative residuals (Figure S3), which shows strong systematic deviations.

Figure 1b compares the time dependencies of the normalized impedance for single-metal MOF-74. First, for all single-metal MOF-74, the adsorption kinetics of water are different from that of MCM-41 silica due to the specific adsorption sites for water in the MOF-74. Second, the adsorption kinetics of the water molecules depend on the metal ion in the MOF-74. This result can be rationalized by considering the different interactions of the water molecules with the metal ions.

Figure 1c,d depicts the sorption kinetics of water for MgxNi(1 − x)-MOF-74 and MgxCo(1 − x)-MOF-74 materials, respectively. In principle, the adsorption kinetics of water in the mixed-metal MOF-74 are comparable to those of the single-metal MOF-74. This concerns, for instance, the three-step adsorption kinetics. However, both figures reveal that the adsorption kinetics depend not only on the type of the metal ion but also on the composition of the mixed-metal MOF-74. The adsorption kinetics of the mixed-metal systems seem to cover a broader time range in comparison to those of the single-metal ones. At first glance, this point can be understood by considering that for the mixed-metal structures, the adsorption sites for water become heterogeneous. As discussed above, the structure of the mixed-metal MOF-74 consists of metal nodes where a specific metal site contains only one kind of metal ion, but a mixture of metal nodes having different metal ions. This composition distribution will lead to a distribution of the adsorption sites for the water molecules, making the time dependence of the adsorption kinetics broader. Unfortunately, no experimental characterization of the heterogeneity of the considered MOF-74 materials is available until now. However, Figure 1c,d reveals that the distribution of the adsorption sites affects the early stages of the adsorption kinetics. This means that, for all mixed-metal MOF-74 structures, the adsorption of water molecules seems to be faster than that for the corresponding single-metal materials. This might be expected, as the early stages of the adsorption kinetics are assigned to the adsorption of water at the OMS. This faster adsorption of water in the mixed-metal MOF-74 materials cannot be rationalized by the time dependence of the adsorption of the single-metal MOFs by a simple two-phase model in series or parallel circuit. Therefore, it is concluded that the hydration of mixed-metal MOF-74 is controlled by additional synergistic effects caused

https://doi.org/10.1021/acs.jpcc.6c02160
J. Phys. Chem. C XXXX, XXX, XXX−XXX

by the different metal nodes and their distribution. These additional effects must be explored in future investigations.

Molecular Fluctuation of Water

To investigate the molecular fluctuations of water inside the pores of the considered MOF-74 materials, broadband dielectric spectroscopy is employed in a wide frequency and temperature range.

Single-Metal MOF-74 Materials

Figure 2a gives the dielectric loss of Mg100-MOF-74 versus frequency and temperature in a 3D representation. The dielectric spectra of all other materials are comparable and given in the Supporting Information in Figure S4. At lower temperatures, at least one relaxation process indicated by a peak is observed. This process is called the w-relaxation (water-relaxation). This relaxation process is followed by a conductivity contribution and conductivity-related effects like Maxwell−Wagner−Sillars (MWS-) and electrode polarization. The w-relaxation process is assigned to molecular fluctuations of water molecules in the pores of the MOF. MWS- and electrode polarization phenomena are parasitic effects due to the blocking of charge carriers at internal phase boundaries (here, most likely grain boundaries) at mesoscopic length scales or at macroscopic length scales at the electrodes. The dielectric behavior of the empty MOF-74 structures considered here as host materials for water was studied in ref 80. Several relaxation processes were observed for the empty dehydrated MOF-74 systems. A relaxation region called process-B was assigned to inward and outward fluctuations of the linkers relative to the pore center, where a further process, process-C, was attributed to small-angle rotational fluctuations of the linker together with corotations of the metal nodes. Figure S5 compares the observed dielectric loss for the dry and the hydrated Ni100-MOF-74 at a temperature of −100 °C (173 K). Although the absolute values of the observed dielectric loss of both materials are probably not correct, the observed dielectric loss for dry Ni100-MOF-74 is by more than an order of magnitude lower than that for the hydrated samples. For the dry Ni100-MOF-74, no relaxation process at the considered temperature is observed. This means that the w-relaxation observed for the hydrated MOFs is not due to the MOF framework but due to the confined water. Moreover, the relaxation processes -B and -C observed for the dry MOF-74 materials are located at much higher temperatures than the w-process (see Figure S6, Supporting Information). Surprisingly, although found for the dry MOF-74 materials, they are not observed as clear peaks in the dielectric spectra for the hydrated samples. On the one hand, it might be argued that these relaxation modes are suppressed by the interaction of water molecules with the frameworks. On the other hand, it might be discussed that the relaxation processes observed for the dry MOF-74 materials are hidden by the conductivity contribution of the hydrated MOF-74 samples.

Figure 2b depicts the dielectric loss at a frequency of 1000 Hz versus the temperature for different cooling and heating runs. There are no significant differences between heating and cooling runs, indicating that no water is desorbed from the pores during the measurement. Furthermore, this proves that the hermetically sealed dielectric cell works properly. Moreover, the agreement of the first cooling and second heating indicates that no significant hydrolysis took place during the dielectric measurements.

Figure 2c compares the dielectric spectra at T = 173 K (−100 °C), especially the w-relaxation for the different single-metal MOF-74 materials with that of MCM-41 silica. For MCM-41 silica, a single peak is observed at ca. 100 Hz, followed by a conductivity contribution at lower frequencies. It is worth noting that the relaxation process due to interfacial water in MCM-41 silica, discussed for instance in ref 48, is not observed in the measurements discussed here. This might be due to a different preparation procedure, including a cleaning step for the pore surface.

The dielectric spectra for the MOF-74 structures are different in at least three aspects compared with those of MCM-41 silica. First, the maximum frequencies of the w-relaxation of the MOF-74 materials are shifted by at least 2 orders of magnitude to higher frequencies in comparison to MCM-41 silica. This might indicate that the structure or morphology of water confined to the pores of MCM-41 silica is different from that in the MOF-74. This issue is discussed in more detail below. Second, the maximum frequency position of the relaxation process depends on the kind of metal ion in the SBU. The behavior evidences that water molecules have different interactions with the different metal ions in the SBUs. Therefore, the w-relaxation process is assigned to water clusters (tetrahedral water) in close-proximity interaction with the metal nodes. Third, especially for Mg100-MOF-74, the peak is followed by a broad plateau region, indicating the presence of further relaxation processes or at least a broader distribution of water states in the considered Mg100-MOF-74 systems. Most likely, the water states range from water interacting strongly with the framework due to interaction with the OMS (water clusters close to the SBU) to liquid-like water. For the Ni100-MOF-74, the plateau-like region is less pronounced compared to that of Mg100-MOF-74. Therefore, it is concluded that Ni100-MOF-74 contains less liquid-like water in comparison to Mg100-MOF-74. This conclusion agrees with experimental results obtained by FTIR spectroscopy.[57] By quantitative analysis of the OH stretching vibration by peak fitting, it was shown that Ni100-MOF-74 contains, at 80% humidity, 25% less liquid-like water than Mg100-MOF-74. For Co100-MOF-74, the plateau is even less pronounced compared to Ni100-MOF-4 and Mg100-MOF-74. Unfortunately, no FTIR investigations are available for the MOF-74 materials containing Co ions. Nevertheless, from the dielectric measurements, it is concluded that Co-MOF-74 might contain the smallest amount of liquid-like water of the considered series of single-metal MOF-74 structures.

It has been proven that the first derivative of the real part of the complex dielectric function versus temperature is sensitive to detecting phase transitions like melting in confined systems.[98,99] A phase transition is indicated by a peak-like discontinuity. Figure 2d compares the derivative $\mathrm{d}(\log \varepsilon')/\mathrm{d}T$ for MCM-41 silica with that of Mg100-MOF-74 at a frequency of 1000 Hz. For MCM-41 silica, a peak-like discontinuity is observed at a temperature of 218 K. This discontinuity evidences a phase transition of confined ice to confined liquid water. This result is also confirmed by differential scanning calorimetry (see Figure S7 in the Supporting Information). There is a further discontinuity at ca. 240 K, which is attributed to the melting of water located at the surfaces of the grains. For Mg100-MOF-74, no discontinuity in the temperature range around 218 K is observed. Therefore, it is concluded that confined water in Mg100-MOF-74 does not undergo a phase transition from confined ice to confined

https://doi.org/10.1021/acs.jpcc.6c02160
J. Phys. Chem. C XXXX, XXX, XXX−XXX

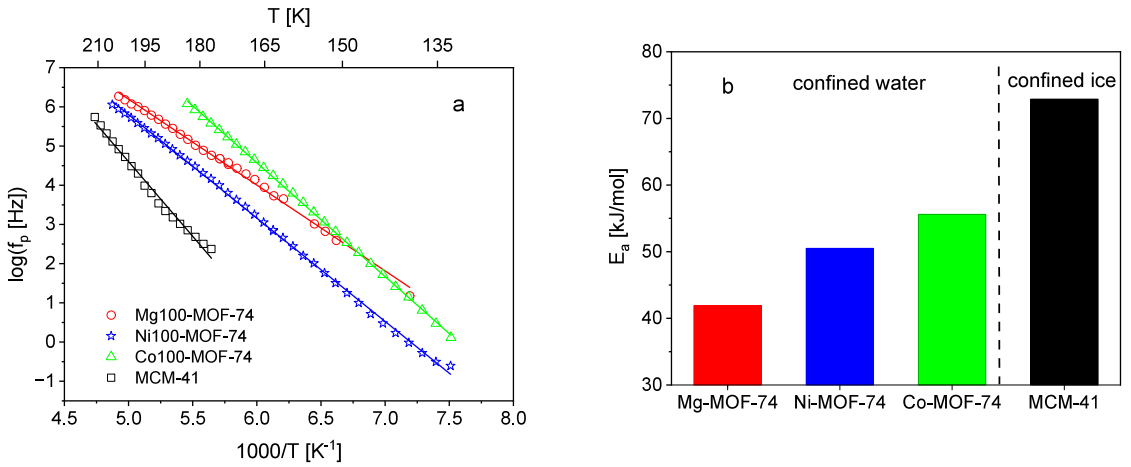

Figure 3. (a) Relaxation rates of the w-relaxation versus inverse temperature: red circles—Mg100-MOF-74, blue asterisk—Ni100-MOF-74, green triangles—Co100-MOF-74, and black squares—MCM-41. Lines are fits of the Arrhenius equation to the corresponding data. (b) Activation energy for the single-metal MOF-74 materials and MCM-41 silica: Red—Mg100-MOF-74, blue—Ni100-MOF-74, green—Co100-MOF-74, and black—MCM-41 silica.

water, and the structure of water is almost in a liquid-like state. This conclusion is further supported by DSC measurements on Mg100-MOF-74 (see Figure S8). No peaks indicating a melting or crystallization of water are observed in the heat flow.

The melting of ice at the surfaces of the grains is also observed as a weak bump for Mg100-MOF-74. A similar behavior is observed for all other considered MOFs. The different behaviors of water in MCM-41 silica and MOF-74 can be discussed in two directions. First, the pores of MCM-41 silica are larger than those of the MOF-74 (see Table 1). The smaller pore sizes of the MOF-74 materials might suppress the crystallization of confined water into confined ice. This conclusion is supported by the experimental observation that water does not crystallize in the pores of MCM-41 silica below a critical pore size.[100] Second, water has different interactions with MCM-41 silica and the MOF-74 materials, which might also suppress the crystallization of confined water for the latter ones. Most probably, both aspects will play a role.

To analyze the dielectric spectra quantitatively, the model function of Havriliak/Negami (HN-function)[101] is fitted to the data.[102] It is given by

$$\varepsilon^*(\omega) = \varepsilon_\infty + \frac{\Delta\varepsilon}{(1 + (i\omega\tau_{HN})^\beta)^\gamma} \quad (2)$$

Here ω denotes the angular frequency $\omega = 2\pi f$. The fractional shape parameters β and γ ($0 < \beta$; $\beta^*\gamma \leq 1$) describe the functional shape of the relaxation spectrum (symmetric and asymmetric broadening) compared to the Debye function. τ_{HN} is the relaxation time of the molecular fluctuations and $\Delta\varepsilon$ expresses the dielectric strength. ε_∞ represents the real part of the complex dielectric function for $\varepsilon_\infty = \lim_{\omega \gg \tau_{HN}^{-1}} \varepsilon'(\omega)$ τ_{HN} is related to the frequency of maximal loss of the relaxation process f_p (relaxation rate) by

$$f_p = \frac{1}{2\pi\tau_{HN}}\left[\sin\frac{\beta\pi}{2 + 2\gamma}\right]^{1/\beta}\left[\sin\frac{\beta\gamma\pi}{2 + 2\gamma}\right]^{-1/\beta} \quad (3)$$

Contributions related to conductivity were treated by adding the term $\frac{\sigma_0}{(\omega^s\varepsilon_0)}$ to the loss part of the HN-function. σ_0 is related to the DC conductivity of the system. The exponent s models non-Ohmic effects in the conductivity ($0 < s \leq 1$), where $s = 1$ holds for Ohmic conductivity. ε_0 is the dielectric permittivity of vacuum.

Figure S9 gives examples of the fits of the HN-function to the dielectric spectra. From the fits, the relaxation rates f_p are estimated and plotted versus inverse temperature for the single-metal MOF-74 in the relaxation map in Figure 3a. The temperature dependence of the relaxation rates of the w-relaxation follows the Arrhenius equation, which is given by

$$f_p = f_\infty \exp\left(-\frac{E_a}{RT}\right) \quad (4)$$

Here E_a is the activation energy, and R is the general gas constant. f_∞ represents the pre-exponential factor denoting the relaxation rates at infinite temperatures. Figure 3b reveals that the values of the activation energy of the w-process depend on the kind of metal ion in the MOF structure. The w-relaxation for Mg100-MOF-74 has, with 41.9 kJ/mol, the lowest value of the activation energy, and that of Co100-MOF-74 with 55.6 kJ/mol the highest value of E_a. The value of the activation energy for Ni100-MOF-74 is 50.5 kJ/mol, in the middle of both former data. The different activation energies reveal the different interactions of the water molecules with the framework. As the different single-metal MOF-74 materials contain different amounts of liquid-like water (see above discussion), in addition to the interactions, one might argue that the different amounts of liquid-like water will influence the molecular fluctuations of water in the water clusters. Above, it was concluded that the amount of liquid-like water decreases from Mg100-MOF-74, versus Ni100-MOF-74, to Co100-MOF-74, which has the lowest amount of liquid-like water. The values of the activation energies of the w-process for the single-metal MOF-74 materials follow the same order. This means, in other words, that Co100-MOF-74 contains the highest amount of tightly bound, which might be the reason for the highest value of the activation energy of the w-process. However, Table 1 reveals that the pore sizes of the different single-metal MOF-74 are quite similar. Therefore, it is concluded that additional geometrical confinement effects for

https://doi.org/10.1021/acs.jpcc.6c02160
J. Phys. Chem. C XXXX, XXX, XXX−XXX

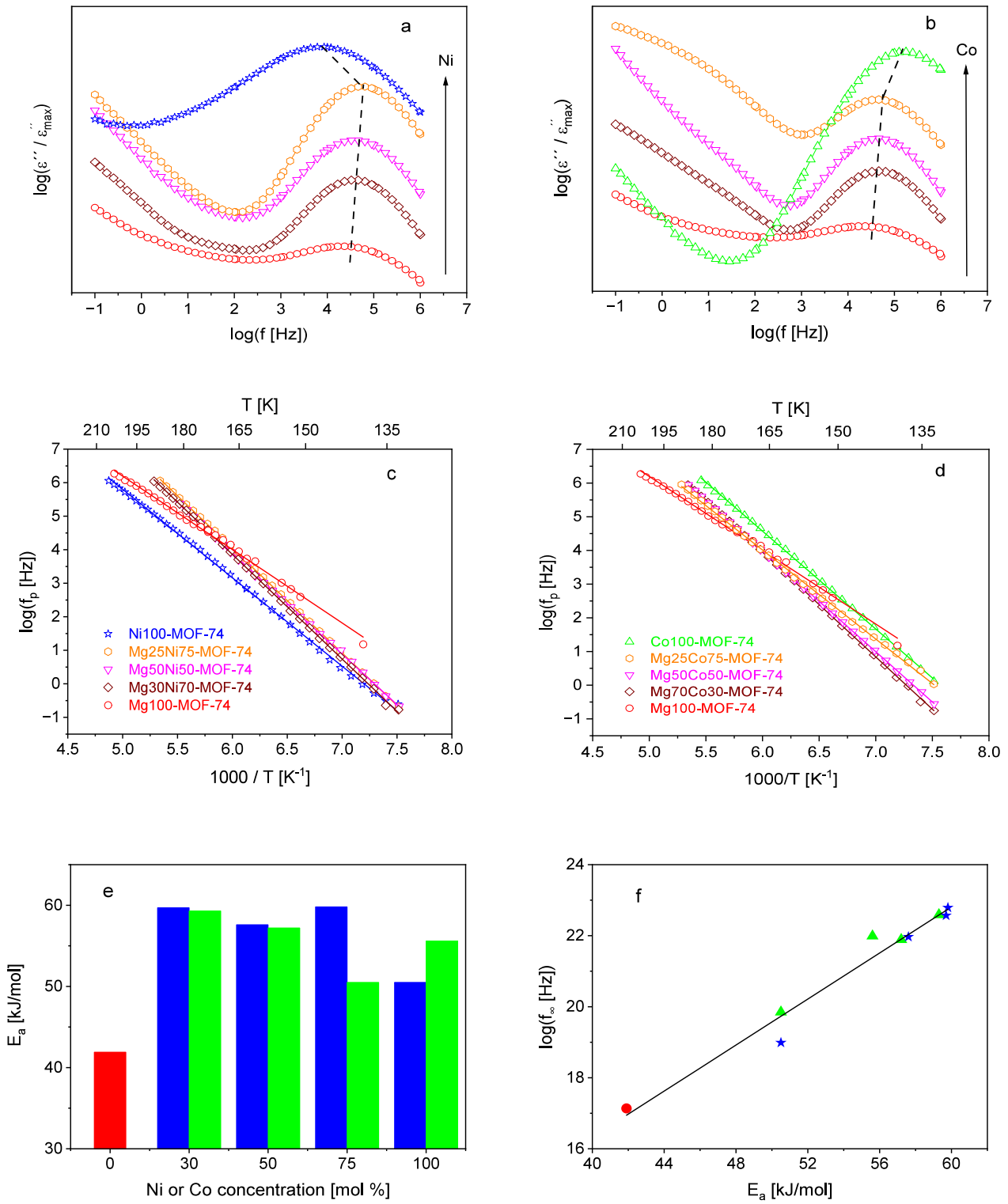

Figure 4. (a) Dielectric loss versus frequency for the Ni-containing MOF-74 materials at a temperature of 173 K (−100 °C): Red circles—Mg100-MOF-74, brown diamonds—Mg70Ni30-MOF-74, pink down-pointing triangles—Mg50Ni50-MOF-74, orange hexagons—Mg25Ni75-MOF-75, and blue asterisks—Ni100-MOF-74. Dashed lines are guides for the eyes. (b) Dielectric loss versus frequency for the Co-containing MOF-74 materials at a temperature of 173 K (−100 °C): Red circles—Mg100-MOF-74, brown diamonds—Mg70Co30-MOF-74, pink down-pointing triangles—Mg50Co50-MOF-74, orange hexagons—Mg25Co75-MOF-75, and green triangles—Co100-MOF-74. Dashed lines are guides for the eyes. (c) Relaxation map for the Ni-containing MOF-74: Red circles—Mg100-MOF-74, brown diamonds—Mg70Ni30-MOF-74, pink down-pointing triangles—Mg50Ni50-MOF-74, orange hexagons—Mg25Ni75-MOF-75, and blue asterisks—Ni100-MOF-74. Lines are fits of the Arrhenius equation to the corresponding data. (d) Relaxation map for the Co-containing MOF-74: Red circles—Mg100-MOF-74, brown diamonds—Mg70Co30-MOF-74, pink down-pointing triangles—Mg50Co50-MOF-74, orange hexagons—Mg25Co75-MOF-75, and green triangles—Co100-MOF-74. Lines are fits of the Arrhenius equation to the corresponding data. (e) Activation energies of the w-relaxation for the considered MOF-74 versus metal concentration: red—Mg100-MOF-74, blue—Ni-ion-containing MOF-74 systems, and green—Co-ion-

https://doi.org/10.1021/acs.jpcc.6c02160
J. Phys. Chem. C XXXX, XXX, XXX−XXX

Figure 4. continued

containing MOF-74. Prefactor f_∞ versus activation energy for the considered MOF-74 in the compensation plot: red—Mg100-MOF-74, blue—Ni-containing MOF-74, and green—Co-containing MOF-74. The line is a linear regression of all data.

the water molecules in the different single-metal MOF-74 materials will play a minor role.

The estimated values of the activation energies might at first glance indicate that the molecular origin of the w-relaxation is localized fluctuations of water. However, at least for Ni100-MOF-74 and Co100-MOF-74, the activation energies seem to be too high for a localized relaxation process. This is further discussed below.

The relaxation rates of the w-relaxation observed for water confined to the pores of MCM-41 silica were too low to be accessed within the available frequency range, and this process could be investigated only in the temperature range where the confined water has the form of confined ice. This interpretation agrees with that given in ref 48. Figure 3b shows that the activation energy of the water molecules in confined ice is much higher than the values of E_a for the w-process of the MOF-74 materials. This again points to a different structure of water confined in the pores of the MOF-74 materials and in MCM-41 silica. As discussed above, the water confined to the MOF-74 has a kind of liquid-like structure, whereas the water in MCM-41 silica is in the state of ice. In this ice-like state, the water molecules have a coordination state of approximately four, which means that each water molecule is, on average, hydrogen-bond coordinated to about four neighboring water molecules, consistent with a tetrahedral network. As discussed above, due to the available frequency range, the temperature range where the water is liquid-like cannot be accessed by these experiments. However, this temperature range can be exceeded by conductivity spectroscopy (see below).

Mixed-Metal MOF-74 Materials

Figure 4a depicts the dielectric loss versus frequency at a temperature of 173 K (−100 °C) for the Ni ion containing MOF-74. The maximum relaxation rate of the w-relaxation depends on the concentration of the Ni ions. At the given temperature, with increasing Ni ion concentration, f_p shifts first to higher frequencies and for Ni100-MOF-74 back to lower frequencies. This seems to be different for the Co-ion-containing systems (see Figure 4b), where the maximum frequency of the maximum of the dielectric loss seems to shift continuously to higher frequencies.

Like for the single-metal MOF-74 systems, the dielectric spectra of the mixed-metal MOF-74 materials were analyzed by fitting the HN function to the data, where, similar to the single-metal MOF-74, the temperature dependence of the relaxation rates of the w-process follows the Arrhenius equation (see Figure 4c for the Ni-ion-containing system and Figure 4d for the Co-ion-containing system). The corresponding activation energies for the mixed-metal MOF-74 are given in Figure 4e and compared to those of the single-metal MOF-74. Besides, for Mg25Co75-MOF-74, the values of the activation energies for the mixed-metal MOF-74 are higher than those for the corresponding single-metal ones. At first glance, this result is difficult to understand, as the interaction of the water molecules with the framework should be comparable to that of the single-metal MOF-74. Nevertheless, it might be hypothesized that the distribution of the metal nodes with different metal ions in the mixed-metal MOF-74 causes further restriction to the molecular fluctuations of the water molecules in the water clusters. It might be argued that the mixed-metal MOF-74 materials contain smaller amounts of liquid-like water, but this is not experimentally proven, especially not for Co-ion-containing MOF-74.

During the estimation of the activation energy, it was found that the prefactors have higher values than expected for a truly localized process, which should be in the order of 10^{12} Hz. The estimated values are higher by several orders of magnitude. Therefore, in Figure 4f the Prefactor f_∞ is plotted versus the activation energy in a kind of compensation plot (Meyer−Neldel plot).[103−105] The Meyer-Neldel (compensation) law, identified across a broad spectrum of thermally activated phenomena, is an empirical relationship in which the Arrhenius Prefactor increases with activation energy, so that $\ln f_\infty$ varies approximately linearly with E_a. It manifests in diverse processes, including diffusive transport, charge-transfer mechanisms in conductive materials, and protein denaturation, among others. A recent compilation can be found elsewhere.[106] Recent work by Thoms and Napolitano has demonstrated that the slow Arrhenius process (SAP) observed in glass-forming materials likewise conforms to the compensation law.[106] The compensation law can be expressed by

$$\ln f_\infty = \ln f_{iso} + \frac{E_a}{RT_{iso}} \tag{5}$$

In this context, T_{iso} denotes the isokinetic temperature at which all relevant processes proceed with an identical characteristic rate f_{iso}.

Figure 4f reveals that the data for the w-relaxation for all considered MOF-74 materials obey a common compensation line. The prevailing view in the literature suggests that the molecular basis of the Meyer−Neldel law arises from the cooperative nature of the underlying molecular fluctuations.[104−108] Therefore, it might be concluded that cooperative effects might be involved in the w-relaxation of the water clusters. As the liquid-like water confined to MCM-41 silica can undergo a glass transition, it might be speculated that this cooperativity is a signature of a glass transition of water confined in the pores of the MOF-74. Because of the Arrhenius-like temperature dependence of the relaxation rates of the w-relaxation and the small pore sizes, the cooperative fluctuations of water in MOF-74 materials might be classified in that case as a hindered glass transition.[109]

To investigate further whether the water confined to MOF-74 undergoes a glass transition, the dielectric strength of the w-relaxation $\Delta\varepsilon$ is considered. The Debye theory of dielectric relaxation, generalized by Fröhlich and Kirkwood, gives for $\Delta\varepsilon$[110]

$$\Delta\varepsilon = \frac{1}{3} g \frac{\mu^2}{k_B T} \frac{N}{V} \tag{6}$$

Where μ^2 denotes the dipole moment associated with the relaxation process under consideration, and N/V represents the number density of the participating dipoles. The parameter g corresponds to the Kirkwood−Fröhlich correlation factor

https://doi.org/10.1021/acs.jpcc.6c02160
J. Phys. Chem. C XXXX, XXX, XXX−XXX

and accounts for static correlations between dipoles. k_B is the Boltzmann constant. For the sake of simplicity, the Onsager reaction field factor, describing internal field effects, is neglected. It is known that for localized relaxation processes, $\Delta\varepsilon$ increases with increasing temperature, whereas for the glass transition, the dielectric strength decreases with increasing temperature.

Figure 5 depicts the temperature dependence of $\Delta\varepsilon$ normalized by its value at the lowest temperature for the single-metal MOF-74 materials. This normalization enables the direct comparison of the dielectric strengths of the different PMO materials. For Mg100-MOF-74, $\Delta\varepsilon$ increases with increasing temperature, whereas for Co100-MOF-74, the dielectric strength decreases with increasing temperature. For Ni100-MOF-74, $\Delta\varepsilon$ seems to be independent of temperature. The temperature dependencies of the w-relaxation for water confined to the different single-metal MOF-74 materials fit into the concept of a hindered glass transition for Mg100-MOF-74; the activation energy of the w-process is relatively low, indicating a more localized process in agreement with the increase of the dielectric strength with increasing temperature.

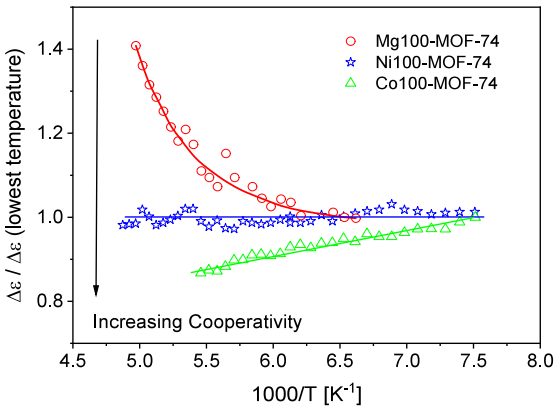

Figure 5. Dielectric strength reduced by its value at the lowest temperature versus inverse temperature: red circles—Mg100-MOF-74, blue asterisks—Ni100-MOF-74, and green triangles—Co100-MOF-74. Lines are guides for the eyes.

With increasing activation energy of the w-relaxation of Ni100-MOF-74 to Co-MOF-74, the temperature dependence of the dielectric strength changes from constant to decreasing with increasing temperature. This behavior indicates an increasing cooperative character of the w-relaxation.

It is important to note that the statement that water undergoes a hindered glass transition should be further proven by additional experiments like fast scanning calorimetry (FSC). It is known that FSC can resolve weak and ill-defined thermal transitions, as expected for a hindered glass transition.[111]

In Figure S10 in the Supporting Information, the data point for the w-process of water confined to the pores of MCM-41 silica is included in the compensation plot. The data point of water confined to the pores of MCM-41 silica does not collapse to the compensation lines established for water confined to the pores of the MOF-74 materials. From that result, it is again concluded that the confined water in the pores of MOF-74 materials and MCM-41 silica behaves fundamentally differently.

Conductivity Analysis of the Dielectric Data

The molecular mobility of confined water is further analyzed by considering the conductivity $\sigma^*(\omega)$. By this approach, molecular mobility can be followed in a broader temperature range by assuming that it is coupled to the conductivity by a slave mechanism. The conductivity is related to the complex dielectric function by

$$\sigma^*(\omega) = \sigma'(\omega) + i\sigma''(\omega) = i\omega\varepsilon_0\varepsilon^*(\omega) \quad (7)$$

where σ' and σ'' are the real and imaginary parts of the complex conductivity. As measurements were carried out on powder, no absolute values of the conductivity could be obtained. Therefore, the observed, measured conductivity σ^*_{obs} is considered. Figure 6a depicts the real part of the complex conductivity for water confined to MCM-41 silica for different temperatures. At high frequencies, the real part of the conductivity, $\sigma'_{obs}(f)$, exhibits a power-law decay as the frequency decreases. This trend continues until $\sigma'_{obs}(f)$ approaches a low-frequency plateau, which corresponds to the direct current (DC) conductivity, $\sigma_{DC,obs}$. From a theoretical perspective, the frequency dependence of $\sigma'(f)$

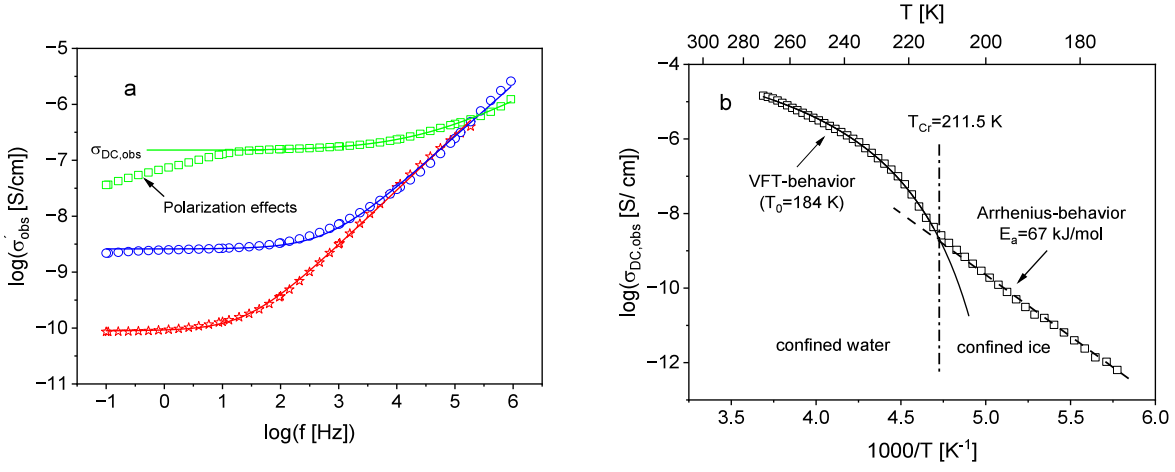

Figure 6. (a) Real part of the observed conductivity σ'_{obs} versus frequency for different temperatures for MCM-41 silica: red asterisks—T = 195.1 K, blue circles—T = 211.1 K, and green squares—T = 225.1 K. Lines are fits of eq 8 to the corresponding data. (b) Observed DC conductivity $\sigma_{DC,obs}$ versus inverse temperature for MCM-41 silica. The solid line is the fit of the VFT equation to the high-temperature data. The dashed line is the fit of the Arrhenius equation to the low-temperature data. The dashed-dotted line indicates the crossover between the low- and high-temperature data.

https://doi.org/10.1021/acs.jpcc.6c02160
J. Phys. Chem. C XXXX, XXX, XXX−XXX

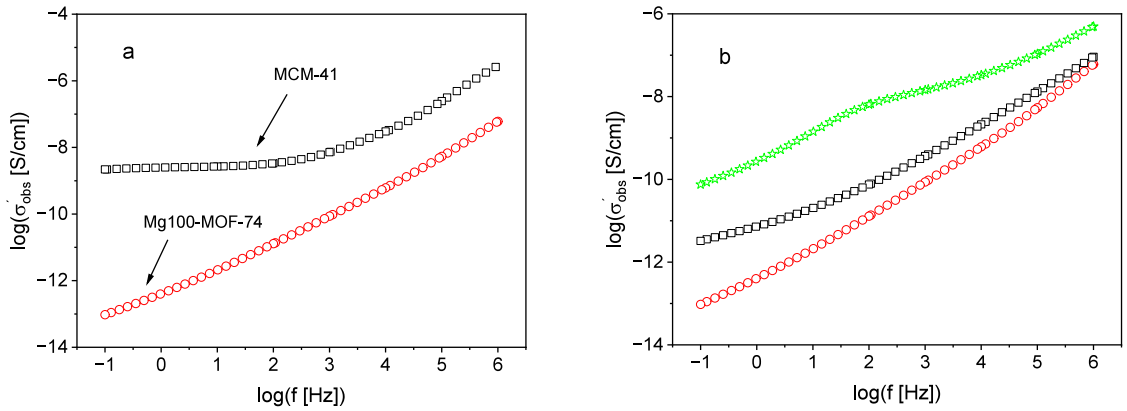

Figure 7. (a) Real part of the observed conductivity σ'_{obs} versus frequency at 211 K: Red circles—Mg100-MOF-74 and black squares—MCM-41 silica. (b) Real part of the observed conductivity σ'_{obs} versus frequency for Mg100-MOF-74 at different temperatures: Read circles—T = 211.1 K, black squares—T = 233.1 K, and green asterisk—T = 273.2 K.

can be rationalized within the framework of the random barrier model.[112] The subsequent decrease in $\sigma'_{obs}(f)$ observed at lower frequencies is attributed to distinct polarization mechanisms: Maxwell−Wagner−Sillars interfacial polarization dominating at intermediate frequencies, and electrode polarization becoming significant in the low-frequency regime.

The DC conductivity is obtained by fitting the empirical Jonscher power-law equation[113] to the frequency-dependent conductivity $\sigma'(f)$, while excluding data affected by polarization phenomena. The Jonscher formula is given by

$$\sigma'(f) = \sigma_{DC}\left(1 + \left(\frac{f}{f_c}\right)^n\right) \tag{8}$$

The exponent n typically assumes values between 0.5 and 1. The characteristic frequency f_c defines the onset of the dispersive regime. Furthermore, the DC conductivity is empirically correlated with f_c via the Barton−Nakajima−Namikawa (BNN) relation.[114]

In Figure 6b, the observed DC conductivity $\sigma_{DC,obs}$ is plotted versus inverse temperature in Arrhenius coordinates. At low temperatures, $\sigma_{DC,obs}(T)$, follows the Arrhenius equation. The estimated activation energy corresponds, with 67 kJ/mol, to the value obtained for the w-process. At ca. T_{cr} = 211.5 K, the temperature of $\sigma_{DC,obs}$ changes from the Arrhenius to the Vogel−Fulcher−Tammann (VFT-) behavior. The VFT equation reads[115−117]

$$\log \sigma_{DC} = \log \sigma_\infty - \frac{A}{T - T_0} \tag{9}$$

A temperature dependence according to the VFT equation indicates glassy dynamics related to a glass transition. Here, the parameter σ_∞ denotes the conductivity at infinite temperatures, where A is a fitting. T_0 is the so-called Vogel or ideal glass transition temperature. For conventional systems, T_0 is found 30−70 K below the thermal glass transition temperature measured by DSC.

Therefore, 242.5 K is defined as the crossover temperature T_{cr}, which corresponds to the temperature where, for MCM-41 silica, the confined ice-like water transforms to confined liquid-like water (see Figure 2d and in the Supporting Information Figure S7). The VFT behavior of the conductivity reveals that the liquid-like water confined to the pores of MCM-41 silica undergoes a glass transition. The Vogel temperature, T_0, is estimated to be 184 K. It should be noted that the crossover in the temperature dependence of the DC conductivity could not be observed in the temperature dependence of the relaxation rates (Figure 3a) due to the restricted available frequency range.

Here, the crossover in the temperature dependence of the DC conductivity is related to the transition of confined ice to confined water. However, in a broader sense, such a transition is also related to a strong-to-fragile transition of confined water, especially for MCM-41 materials with smaller pore sizes where water cannot crystallize (see, for instance, ref 118 and references cited there).

Figure 7a compares the real part of the observed complex conductivity for MCM-41 with that of Mg-MOF-74 at the same temperature (T = 211.1 K). In contrast to the data of MCM-41 silica, for Mg100-MOF-74, no plateau region that indicates a DC conductivity is observed. That no DC conductivity can be extracted stays true for the highest temperatures (T = 273 K, see Figure 7b). For all temperatures, the frequency dependence of the real part of the complex conductivity is overlaid by strong polarization effects. As the grain sizes of MCM-41 silica and Mg100-MOF-74 are comparable, it is concluded that the origin of the pronounced polarization for Mg100-MOF-74 is a Maxwell−Wagner-Sillars polarization, which takes place at shorter length scales. It might be discussed that the charge carriers are blocked within the framework itself. One might discuss that the charge carriers are blocked at the metal sites. For all other MOF-74 systems, a comparable frequency dependence of the real part of the complex conductivity is observed.

CONCLUSIONS

In this work, we systematically investigated the hydration kinetics and molecular fluctuations of water confined in a comprehensive series of MOF-74 materials containing Mg, Ni, and Co ions and mixed-metal compositions. By combining in situ impedance spectroscopy with broadband dielectric spectroscopy, we obtained a detailed molecular-level picture of how water interacts with and dynamically responds within these microporous host systems. This includes the hydration kinetics.

The hydration experiments demonstrate that water sorption in MOF-74 proceeds through a distinct multistep mechanism that differs fundamentally from that of mesoporous MCM-41

https://doi.org/10.1021/acs.jpcc.6c02160
J. Phys. Chem. C XXXX, XXX, XXX−XXX

silica. The presence of coordinatively unsaturated OMS in MOF-74 introduces an initial fast adsorption step associated with strong coordinative binding. This is followed by the formation of hydrogen-bonded water clusters in the vicinity of the metal nodes and finally by a kind of capillary condensation, leading to complete pore filling. Mixed-metal MOF-74 systems exhibit accelerated and broadened sorption kinetics compared to their single-metal analogues, reflecting the heterogeneous distribution of metal nodes and thus a broader distribution of adsorption sites.

Broadband dielectric spectroscopy revealed a well-defined water-specific relaxation process (w-relaxation) for all the MOF-74 samples. This process can be assigned to the molecular fluctuations within water clusters close to the coordinatively bonded water at the OMS. The temperature dependence of the relaxation rates of the w-relaxation follows Arrhenius behavior with activation energies strongly dependent on the identity and ratio of the metal ions. In single-metal MOFs, activation energies increase in the order Mg < Ni < Co, consistent with spectral signatures indicating decreasing amounts of liquid-like water from Mg- to Co-based systems. Here, liquid-like water means that it is not strongly bonded to the framework. Remarkably, the activation energies for mixed-metal MOF-74 materials are higher than those of the corresponding single-metal frameworks, suggesting that the heterogeneous local environment imposes an additional hindrance on the molecular mobility of confined water.

A key finding is that, unlike in MCM-41 silica, water confined in MOF-74 remains liquid-like across the entire studied temperature range and does not exhibit a melting transition. This difference can be attributed to both the smaller pore size of MOF-74 and the strong local interactions between water and the metal nodes, both of which inhibit the nucleation of ice-like structures.

The compensation (Meyer−Neldel) analysis provides insight into the cooperative nature of the confined water dynamics. All MOF-74 systems, regardless of the metal identity or composition, collapse onto a common compensation line. This behavior is indicative of cooperative molecular motions and supports the interpretation that the w-relaxation might correspond to a hindered glass-transition-like process of water clusters under confinement. In contrast, water in MCM-41 silica does not follow this compensation relationship, reinforcing the fundamentally different structural and dynamical states induced by confinement in MOF-74.

Overall, this study highlights the critical role of pore chemistry and metal composition in governing hydration behavior and molecular mobility in microporous materials. The combination of strongly interacting OMS, narrow pore geometry, and tunable mixed-metal environments in MOF-74 creates a rich landscape of confined water states that can be modulated in a predictable manner. These insights provide a foundation for the rational design of MOF-based materials for applications involving water transport, sorption, or reactivity, including catalysis, separations, and energy-related technologies.

■ ASSOCIATED CONTENT

Supporting Information

The Supporting Information is available free of charge at https://pubs.acs.org/doi/10.1021/acs.jpcc.6c02160.

Photo of the humidity chamber; dielectric spectra versus frequency and temperature in 3D representations for all investigated materials; comparison of the temperature dependence of the relaxation processes of the dry and hydrated Mg100-MOF-74, DSC measurements for MCM-41 silica, example of the fitting of the HH-function; compensation plot including the data set of MCM-41 silica (PDF)

■ AUTHOR INFORMATION

Corresponding Authors

Michael Fröba − *Institute of Inorganic and Applied Chemistry, University of Hamburg, 20146 Hamburg, Germany*; Email: Michael.Froeba@uni-hamburg.de

Patrick Huber − *Institute for Materials and X-ray Physics, Hamburg University of Technology, 21073 Hamburg, Germany; Centre for X-ray and Nano Science CXNS, Deutsches Elektronen-Synchrotron DESY, 22607 Hamburg, Germany*; orcid.org/0000-0002-2126-9100; Email: Patrick.Huber@tuhh.de

Andreas Schönhals − *Bundesanstalt für Materialforschung und -prüfung (BAM), 12205 Berlin, Germany; Institut für Chemie, Technische Universität Berlin, 10623 Berlin, Germany*; orcid.org/0000-0003-4330-9107; Email: Andreas.Schoenhals@bam.de

Authors

Arda Yildirim − *Bundesanstalt für Materialforschung und -prüfung (BAM), 12205 Berlin, Germany; Institute for Materials and X-ray Physics, Hamburg University of Technology, 21073 Hamburg, Germany; Centre for X-ray and Nano Science CXNS, Deutsches Elektronen-Synchrotron DESY, 22607 Hamburg, Germany;* Present Address: One.five GmbH, Reichkanzlerstraße 2a, 22609 Hamburg, Germany

Paulina Szymoniak − *Bundesanstalt für Materialforschung und -prüfung (BAM), 12205 Berlin, Germany*; orcid.org/0000-0003-2152-5095

Tabea C. V. Haug − *Institute of Inorganic and Applied Chemistry, University of Hamburg, 20146 Hamburg, Germany*

Complete contact information is available at: https://pubs.acs.org/10.1021/acs.jpcc.6c02160

Notes

The authors declare no competing financial interest.

■ ACKNOWLEDGMENTS

We acknowledge the scientific exchange with the Centre for Molecular Water Science (CMWS). This work was supported in the frame of the LFF project 'Control of the special properties of water in nanopores' (LFF-FV68-2019), financed by the BWFGB as well as by the DFG as part of the Excellence Strategy of the Federal Government and the federal states - EXC 3120/1 BlueMat: Water-Driven Materials − 533771286.

■ REFERENCES

(1) Ball, P. Water as an Active Constituent in Cell Biology. *Chem. Rev.* **2008**, *108*, 74−108.

(2) Ball, P. Water — an enduring mystery. *Nature* **2008**, *452*, 291−292.

(3) Zanotti, J. M.; Gibrat, G.; Bellissent-Funel, M. C. Hydration water rotational motion as a source of configurational entropy driving protein dynamics. Crossovers at 150 and 220 K. *Phys. Chem. Chem. Phys.* **2008**, *10*, 4865.
(4) Malikova, N.; Longeville, S.; Zanotti, J. M.; Dubois, E.; Marry, V.; Turq, P.; Ollivier, J. Signature of Low-Dimensional Diffusion in Complex Systems *Phys. Rev. Lett.* **2008**, *101*, No. 265901.
(5) Bagchi, B. Water Dynamics in the Hydration Layer around Proteins and Micelles. *Chem. Rev.* **2005**, *105*, 3197.
(6) Maurel, C.; Reizer, J.; Schroeder, J. I.; Chrispeels, M. J. The vacuolar membrane protein gamma-TIP creates water specific channels in Xenopus oocytes. *EMBO J.* **1993**, *12*, 2241−2247.
(7) Preston, G. M.; Carroll, T. P.; Guggino, W. B.; Agre, P. Appearance of water channels in Xenopus oocytes expressing red cell CHIP28 protein. *Science* **1992**, *256*, 385−387.
(8) Sui, H.; Han, B.-G.; Lee, J. K.; Walian, P.; Jap, B. K. Structural basis of water-specific transport through the AQP1 water channel. *Nature* **2001**, *414*, 872−878.
(9) Swenson, J.; Bergman, R.; Howells, W. S. Quasielastic neutron scattering of two-dimensional water in a vermiculite clay. *J. Chem. Phys.* **2000**, *113*, 2873.
(10) Malikova, N.; Longeville, S.; Zanotti, J. M.; Dubois, E.; Marry, V.; Turq, P. Signature of Low-Dimensional Diffusion in Complex Systems. *Phys. Rev. Lett.* **2008**, *101*, No. 265901.
(11) Marry, V.; Dubois, E.; Malikova, N.; Durand-Vidal, S.; Longeville, S.; Breu, J. Water Dynamics in Hectorite Clays: Influence of Temperature Studied by Coupling Neutron Spin Echo and Molecular Dynamics. *Environ. Sci. Technol.* **2011**, *45*, 2850.
(12) Taillefert, M.; Neuhuber, S.; Bristow, G. The effect of tidal forcing on biogeochemical processes in intertidal salt marsh sediments. *Geochem. Trans.* **2007**, *8*, 6.
(13) Huber, P. Soft matter in hard confinement: phase transition, thermodynamics, structure, texture diffusion and flow in nanoporous media. *J. of Physics: Condensed Matter* **2015**, *27*, No. 103102.
(14) Hugo, K. C. Confinement effects on freezing and melting. *J. Phys.: Condens. Matter* **2001**, *13*, R95−R133.
(15) Dong, S.; Leng, J.; Feng, Y.; Liu, M.; Stackhouse, C. J.; Schönhals, A.; Chiappisi, L.; Gao, L.; Chen, W.; Shang, J.; Jin, L.; Qi, Z.; Schalley, C. A. Structural water as an essential comonomer in supramolecular polymerization. *Sci. Adv.* **2017**, *3*, No. eaao0900.
(16) Xu, Q.; Szymoniak, P.; Kolmangadi, M. A.; Yang, Z.; Wang, S.; Gao, Y.; Shang, J.; Hunger, J.; Aldiyarov, A.; Schönhals, A.; Ge, Y.; Qi, Z. Molecular engineering of a supramolecular polymer adhesive with confined water and a single crown ether. *Chem. Sci.* **2025**, *16*, 1995−2003.
(17) Debenedetti, P. G. Supercooled and glassy water. *J. Phys.: Condens. Matter* **2003**, *15*, R1669−R1726.
(18) Coin, F.; di Lisio, V.; Cangialosi, D.; Cerveny, S. The glass transition and the dynamics of water within pectin and metal-organic framework nanochannels. *J. Chem. Phys.* **2025**, *163*, 164507.
(19) Li, Y.; Wang, S.; Xiao, Z.; Leng, J.; Zhang, Z.; Gao, T.; Tang, Z. Enhancing Li-ion transport in solid electrolytes by confined water. *Smal* **2022**, *18*, No. e2201094.
(20) Coudert, F.-X.; Boutin, A.; Fuchs, A. H. Open questions on water confined in nanoporous materials. *Commun. Chem.* **2021**, *4*, 106.
(21) Brinker, M.; Huber, P. Wafer-Scale Electroactive Nanoporous Silicon: Large and Fully Reversible Electrochemo-Mechanical Actuation in Aqueous Electrolytes. *Adv. Mater.* **2022**, *34*, No. e2105923.
(22) Bartolomé, L.; Verziaggi, N.; Brinker, M.; Amayuelas, E.; Merchori, S.; Arkan, M. Z.; Eglitis, R.; Šutka, A.; Chorążewski, M.; Huber, P.; Meloni, S.; Grosu, Y. Triboelectrification during non-wetting liquids intrusion−extrusion in hydrophobic nanoporous silicon monoliths. *Nano Energy* **2025**, *146*, No. 111488.
(23) Knight, A. W.; Kalugin, N. G.; Coker, E.; Ilgen, A. G. Water properties under nano-scale confnement. *Sci. Rep.* **2019**, *9*, 8246.
(24) Hedström, J.; Swenson, J.; Bergman, R.; Jansson, H.; Kittaka, S. Does confined water exhibit a fragile-to-strong transition? *Eur. Phys. J.: Spec. Top.* **2007**, *141*, 53−56.
(25) Lederle, C.; Sattig, M.; Vogel, M. Effects of partial crystallization on the dynamics of water in mesoporous silica. *J. Phys. Chem. C* **2018**, *122*, 15427−15434.
(26) Sjöström, J.; Swenson, J.; Bergman, R.; Kittaka, S. Investigating hydration dependence of dynamics of confined water: Monolayer, hydration water and Maxwell−Wagner processes. *J. Chem. Phys.* **2008**, *128*, 154503.
(27) Sattig, M.; Vogel, M. Dynamic crossovers and stepwise solidification of confined water: H-2 NMR study. *J. Phys. Chem. Lett.* **2014**, *5*, 174−178.
(28) Sattig, M.; Reutter, S.; Fujara, F.; Werner, M.; Buntkowsky, G.; Vogel, M. NMR studies on the temperature-dependent dynamics of confined water. *Phys. Chem. Chem. Phys.* **2014**, *16*, 19229−19240.
(29) Liu, L.; Chen, S.-H.; Faraone, A.; Yen, C.-W.; Mou, C.-Y. Pressure dependence of fragile-to-strong transition and a possible second critical point in Supercooled confined water. *Phys. Rev. Lett.* **2005**, *95*, No. 117802.
(30) Swenson, J.; Cerveny, S. Dynamics of deeply Supercooled interfacial water. *J. Phys.: Condens. Matter* **2015**, *27*, No. 033102.
(31) Weigler, M.; Brodrecht, M.; Buntkowsky, G.; Vogel, M. Reorientation of deeply cooled water in mesoporous silica: NMR studies of the pore-size dependence. *J. Phys. Chem. B* **2019**, *123*, 2123−2134.
(32) Frunza, L.; Schönhals, A.; Kosslick, H.; Frunza, S. Relaxation processes of water confined to AlMCM-41 molecular sieves. Influence of the hydroxyl groups of the pore surface. *Eur. Phys. J. E* **2008**, *26*, 379−386.
(33) Soper, A. K. Density profile of water confined in cylindrical pores in MCM-41 silica. *J. Phys.: Condens. Matter* **2012**, *24*, 064107.
(34) Grünberg, B.; Emmler, T.; Gedat, E.; Shenderovich, I.; Findenegg, G. H.; Limbach, H.-H.; Buntkowsky, G. Hydrogen Bonding of Water Confined in Mesoporous Silica MCM-41 and SBA-15 Studied by ^{1}H Solid-State NMR. *Chem. −A Eur. J.* **2004**, *10*, 5689−5696.
(35) Frunza, L.; Kosslick, H.; Pitsch, I.; Frunza, S.; Schönhals, A. Rotational fluctuations of water inside the nanopores of SBA-type molecular sieves. *J. Phys. Chem. B* **2005**, *109*, 9154−9159.
(36) Kiwilsza, A.; Pajzderska, A.; Gonzales, M. G.; Mielcarek, J.; Wasicki, J. QENS and NMR Study of Water Dynamics in SBA-15 with a Low Water Content. *J. Phys. Chem. C* **2015**, *119*, 16578−16586.
(37) Suzuki, Y.; Steinhart, M.; Graf, R.; Butt, H.-J.; Floudas, G. Dynamics of ice/water confined in nanoporous alumina. *J. Phys. Chem. B* **2015**, *119*, 14814−14820.
(38) Gor, G. Y.; Bertinetti, L.; Bernstein, N.; Hofmann, T.; Fratzl, P.; Huber, P. Elastic response of mesoporous silicon to capillary pressures in the pores. *Appl. Phys. Lett.* **2015**, *106*, 261901.
(39) Jansson, H.; Swenson, J. Dynamics of water in molecular sieves by dielectric spectroscopy. *Eur. Phys. J. E: Soft Matter* **2003**, *12*, 51−54.
(40) Yao, Y.; Fella, V.; Huang, W.; Zhang, K.A. I.; Landfester, K.; Butt, H.-J.; Vogel, M.; Floudas, G. Crystallization and dynamics of water confined in model mesoporous silica particles: Two ice nuclei and two fractions of water. *Langmuir* **2019**, *35*, 5890−5901.
(41) Melillo, J. H.; Cangialosi, D.; Di Lisio, V.; Steinrücken, E.; Vogel, M.; Cerveny, S. Complexity of confined water vitrification and its glass transition temperature. *Proc. Natl. Acad. Sci. U. S. A.* **2024**, *121*, No. e2407030121.
(42) Pahlke, B. H.; Lusceac, S. A.; Geil, B.; Fujara, F. NMR study of local and long range dynamics of adsorbed water in zeolite NaY(Br). *Z. Phys. Chem.* **2012**, *226*, 1093−1113.
(43) Frunza, L.; Kosslick, H.; Frunza, S.; Schönhals, A. Unusual relaxation behavior of water inside the sodalite cages of faujasite-type molecular sieves. *J. Phys. Chem. B* **2002**, *106*, 9191.

https://doi.org/10.1021/acs.jpcc.6c02160
J. Phys. Chem. C XXXX, XXX, XXX−XXX

(44) Cerveny, S.; Barroso-Bujans, F.; Alegría, Á.; Colmenero, J. Dynamics of water intercalated in graphite oxide. *J. Phys. Chem. C* **2010**, *114*, 2604−2612.
(45) Gießelmann, N. C.; Lenz, P.; Meinert, S.-M.; Simon, T.; Jo, W.; Striker, N. N.; Fröba, M.; Lehmkühler, F. Structure of water under confinement in periodic organosilicas. *J. Phys. Chem. C* **2024**, *128*, 499−507.
(46) Jani, A.; Busch, M.; Mietner, J. B.; Ollivier, J.; Appel, M.; Frick, B.; Zanotti, J.-M.; Ghoufi, A.; Huber, P.; Fröba, M.; Morineau, D. Dynamics of water confined in mesopores with variable surface interaction. *J. Chem. Phys.* **2021**, *154*, No. 094505.
(47) Mietner, B. J.; Fröba, M.; Valiullin, R. Water transport in periodic mesoporous organosilica materials. *J. Phys. Chem. C* **2018**, *122*, 12673.
(48) Malfait, B.; Jani, A.; Mietner, J. B.; Lefort, R.; Huber, P.; Fröba, M.; Morineau, D. Influence of Pore Surface Chemistry on the Rotational Dynamics of Nanoconfined Water. *J. Phys. Chem. C* **2021**, *125*, 16864.
(49) Lenz, P.; Meinert, S.-M.; König, S.; Steiger, M.; Fröba, M. Influence of Surface chemistry on t-layer dimension and density of Nanoconfined water be fine-tunning the functional groups of periodic mesoporous organosilicas. *J. Phys. Chem. C* **2025**, *129*, 12536−12550.
(50) Lenz, P.; Sazama, U.; Steiger, M.; Fröba, M. Periodic mesoporous organosilicas as host materials for studying surface chemistry effects on the freezing and melting behavior of non-oconfined water. *J. Phys. Chem. C* **2025**, *129*, 20373−20386.
(51) Lenz, P.; Sazama, U.; König, S.; Steiger, M.; Fröba, M. The role of fine-tuned surface functionality on adsorption thermodynamics of Nanoconfined water within periodic mesoporous organosilicas. *J. Phys. Chem. C* **2026**, *130*, 3472.
(52) Mozdehei, A.; Lenz, P.; Gries, S.; Meinert, S.-M.; Lefort, R.; Zanotti, J.-M.; Berrod, Q.; Appelt, M.; Busch, M.; Huber, P.; Fröba, M. Colossal effect of nanopore surface ionic charge on the dynamics of confined water. *J. Phys. Chem. C* **2025**, *129*, 18311−18324.
(53) Mietner, J. B.; Brieler, F. J.; Lee, Y. J.; Fröba, M. Properties of water confined in periodic mesoporous organosilicas − nanoimprintig the local structure. *Angew. Chem., Int. Ed.* **2017**, *56*, 12348−12351.
(54) Gießelmann, N. C.; Lenz, P.; Meinert, S.-M.; Simon, T.; Bauer, R. P. C.; Jo, W.; Claas, S.; Köhn, C.; Striker, N. N.; Fröba, M.; Lehmkühler, F. The structure of ice under confinement in periodic mesoporous organosilicas (PMOs). *J. Chem. Phys.* **2024**, *161*, No. 034508.
(55) Malfait, B.; Moréac, A.; Jani, A.; Lefort, R.; Huber, P.; Fröba, M.; Morineau, D. Structure of Water at Hydrophilic and Hydrophobic Interfaces: Raman Spectroscopy of Water Confined in Periodic Mesoporous (Organo)Silicas. *J. Phys. Chem. C* **2022**, *126*, 3520.
(56) Fischer, J. K. H.; Sippel, P.; Denysenko, D.; Lunkenheimer, P.; Volkmer, D.; Loidl, A. Supercooled water confined in a metal-organic framework. *Commun. Phys.* **2020**, *3*, 95.
(57) Haug, T. C. V.; Hoffmann, F.; Tasova, M. N.; Heffels, R.; Fröba, M. IR spectroscopic studies on water confined in an isoreticular MOF series − Influence of the metal and liker functionality. *Adv. Mater. Interfaces* **2025**, *12*, No. 2400847.
(58) Furukawa, H.; Cordova, K. E.; O'Keeffe, M.; Yaghi, O. M. The chemistry and applications of metal-organic frameworks. *Science* **2013**, *341*, No. 1230444.
(59) Yaghi, O. M.; O'Keeffe, M.; Ockwig, N. W.; Chae, H. K.; Eddaoudi, M.; Kim, J. Reticular synthesis and the design of new materials. *Nature* **2003**, *423*, 705−714.
(60) Freund, R.; Zaremba, O.; Arnauts, G.; Ameloot, R.; Skorupskii, G.; Dinca, M.; Bavykina, A.; Gascon, J.; Ejsmont, A.; Goscianska, J.; Kalmutzki, M.; Laechelt, U.; Ploetz, E.; Diercks, C. S.; Wuttke, S. The current status of MOF and COF applications. *Angew. Chem., Int. Ed.* **2021**, *60*, 23975−24001.
(61) Stock, N.; Biswas, S. Synthesis of Metal-Organic Frameworks (MOFs): Routes to Various MOF Topologies, Morphologies, and Composites. *Chem. Rev.* **2012**, *112*, 933−969.
(62) James, S. L. Metal-organic frameworks. *Chem. Soc. Rev.* **2003**, *32*, 276.
(63) Kapelewski, M. T.; Geier, S. J.; Hudson, M. R.; Stück, D.; Mason, J. A.; Nelson, J. N.; Xiao, D. J.; Hulvey, Z.; Gilmour, E.; FitzGerald, S. A.; Head-Gordon, M.; Brown, C. M.; Long, J. R. M_2(m-dobdc) (M = Mg, Mn, Fe, Co, Ni) Metal−Organic Frameworks Exhibiting Increased Charge Density and Enhanced H_2 Binding at the Open Metal Sites. *J. Am. Chem. Soc.* **2014**, *136*, 12119−12129.
(64) Kreno, L. E.; Leong, K.; Farha, O. K.; Allendorf, M.; Van Duyne, R. P.; Hupp, J. T. Metal−Organic Framework Materials as Chemical Sensors. *Chem. Rev.* **2012**, *112*, 1105−1125.
(65) Marco-Lozar, J. P.; Juan-Juan, J.; Suárez-García, F.; Cazorla-Amorós, D.; Linares-Solano, A. MOF-5 and activated carbons as adsorbents for gas storage. *Int. J. Hydrogen Energy* **2012**, *37*, 2370−2381.
(66) Szcześniak, B.; Choma, J.; Jaroniec, M. Gas adsorption properties of hybrid graphene−MOF materials. *J. Colloid Interface Sci.* **2018**, *514*, 801−813.
(67) Mirzaei, S.; LotfiKatooli, L.; Ahmadpour, A.; Niknam Shahrak, M.; Haghbin, M. R.; Arami-Niya, A. Development of a novel porous adsorbent based on metal−organic frameworks for efficient CO_2 capture and storage. *Chem. Eng. Res. Des.* **2024**, *203*, 419−430.
(68) Oh, H.; Maurer, S.; Balderas-Xicohtencatl, R.; Arnold, L.; Magdysyuk, O. V.; Schütz, G.; Müller, U.; Hirscher, M. Efficient synthesis for large-scale production and characterization for hydrogen storage of ligand exchanged MOF-74/174/184-M (M = Mg^{2+}, Ni^{2+}). *Int. J. Hydrog. Energy* **2017**, *42*, 1027−1035.
(69) Kalmutzki, M. J.; Diercks, C. S.; Yaghi, O. M. Metal−Organic Frameworks for Water Harvesting from Air. *Adv. Mater.* **2018**, *30*, No. 1704304.
(70) Ma, A.; Cong, H.; Deng, H. Multivariate MOF for optimizing atmospheric water harvesting. *Green Energy Environ.* **2022**, *7*, 575−577.
(71) Huang, X.; Qin, Q.; Ma, Q.; Wang, B. Atmospheric Water Harvesting with Metal−Organic Frameworks and Their Composites: From Materials to Devices. *Water* **2022**, *14*, 3487.
(72) Arabbaghi, E. K.; Mokhtari, J.; Naimi-Jamal, M. R.; Khosravi, A. Metal−organic frameworks as advanced adsorbents for gas storage and separation: A review. *J. Porous Mater.* **2021**, *28*, 641.
(73) Hu, J.; Chen, Y.; Zhang, H.; Chen, Z. Metal−organic frameworks for gas adsorption and separation: Recent advances and perspectives. *Solid State Chem.* **2021**, *294*, No. 121853.
(74) Cao, J.; Li, X.; Tian, H. Metal−Organic Frameworks for Biomedical Applications. *Curr. Med. Chem.* **2020**, *27*, 5949.
(75) Dietzel, P. D. C.; Blom, R.; Fjellvåg, H. Base-Induced Formation of Two Magnesium Metal-Organic Framework Compounds with a Bifunctional Tetratopic Ligand. *Eur. J. Inorg. Chem.* **2008**, *2008*, 3624.
(76) Howe, J. D.; Morelock, C. R.; Jiao, Y.; Chapman, K. W.; Walton, K. S.; Sholl, D. S. Understanding structure, metal distribution and water adsorption in mixed-metal MOF-74. *J. Phys. Chem. C* **2017**, *121*, 627−635.
(77) Ji, Z.; Li, T.; Yaghi, O. M. Sequencing of metals in multivariate metal-organic frameworks. *Science* **2020**, *369*, 674−780.
(78) Glover, T. G.; Peterson, G. W.; Schindler, B. J.; Britt, D.; Yaghi, O. MOF-74 building unit has a direct impact on toxic gas adsorption. *Chem. Eng. Sci.* **2011**, *66*, 163−170.
(79) Jiao, Y.; Morelock, C. R.; Burtch, N. C.; Mounfield, W. P.; Hungerford, J. T.; Walton, K. S. Tuning the kinetic water stability and adsorption interactions of Mg-MOF-74 by partial substitution with Co or Ni. *Ind. Eng. Chem. Res.* **2015**, *54*, 12408−12414.
(80) Yildirim, A.; Haug, T. C. V.; Fröba, M.; Huber, P.; Schönhals, A. Molecular Fluctuations in Mixed-Metal MOF-74: Influence of the Metal Composition. *RCS. Advances* **2025**, *15*, 29109−29118.
(81) Kremer, F.; Schönhals, A. Broadband dielectric measurement techniques. In *Broadband Dielectric Spectroscopy*, Kremer, F.; Schönhals, A., Eds.; Springer: Berlin, 2003; pp 36−57.
(82) Roy, S.; Richert, R. Dielectric spectroscopy study of myoglobin in glycerol−water mixtures. *Biochim. Biophys. Acta* **2024**, *1844*, 323−329.

https://doi.org/10.1021/acs.jpcc.6c02160
J. Phys. Chem. C XXXX, XXX, XXX−XXX

(83) Kloß, M.; Beerbaum, M.; Baier, D.; Weinberger, C.; Zysk, F.; Elgabarty, H.; Kühne, Th. D.; Tiemann, M. Understanding the hydration in COP-27 metal-organic frameworks: Strong impact of the chemical nature of the metal (Cu, Zn). *Adv. Mater. Interfaces* **2024**, *11*, No. 2400476.
(84) Ojha, D.; Karhan, K.; Kühne, T. D. On the Hydrogen Bond Strength and Vibrational Spectroscopy of Liquid Water. *Sci. Rep.* **2018**, *8*, 16888.
(85) Møller, K. B.; Rey, R.; Hynes, J. T. Hydrogen bond dynamics in water and ultrafast infrared spectroscopy: A theoretical study. *J. Phys. Chem. A* **2004**, *108*, 1275.
(86) Ohno, K.; Okimura, M.; Akai, N.; Katsumoto, Y. Hydrogen bonding in water studied by vibrational spectroscopy and quantum chemical calculations. *Phys. Chem. Chem. Phys.* **2005**, *7*, 3005.
(87) Tainter, C. J.; Ni, Y.; Shi, L.; Skinner, J. L. Orientational Correlation Function for Water from Molecular Dynamics Simulations: Reinterpretation of Experimental Results. *J. Phys. Chem. Lett.* **2013**, *4*, 12.
(88) Jain, T. K.; Varshney, M.; Maitra, A. Structural Studies of Aerosol OT Reverse Micellar Aggregates by FT-IR Spectroscopy. *J. Phys. Chem.* **1989**, *93*, 7409.
(89) Onori, G.; Santucci, A. Infrared Study of Hydrogen Bonding in Water Confined in Reverse Micelles. *J. Phys. Chem.* **1993**, *97*, 5430.
(90) Le Caër, S.; Pin, S.; Esnouf, S.; Raffy, Q.; Renault, J. P.; Brubach, J. B.; Creff, G.; Roy, P. Radiolysis of water confined in porous silica: A combined experimental and theoretical study. *Phys. Chem. Chem. Phys.* **2011**, *13*, 17658.
(91) Knight, A. W.; Kalugin, N. G.; Coker, E.; Ilgen, A. G. Water properties under nano-scale confinement. *Sci. Rep.* **2019**, *9*, 8246.
(92) Dietzel, P. D. C.; Johnsen, R. E.; Blom, R.; Fjellvåg, H. Structural Changes and Coordinatively Unsaturated Metal Atoms on Dehydration of Honeycomb Analogous Microporous Metal−Organic Frameworks. *Chem.—Eur. J.* **2008**, *14*, 2389.
(93) Kremer, F.; Schönhals, A. Broadband dielectric measurement techniques (10^{-6} Hz to 10^{12} Hz). In *Broadband Dielectric Spectroscopy*; Kremer, F.; Schönhals, A., Eds.; Springer: Berlin, Heidelberg, 2003; pp 35−58.
(94) Andrić, J. M.; Janjić, V. G.; Ninković, D. B.; Zarić, S. D. The influence of water molecule coordination to a metal ion on water hydrogen bonds. *Phys. Chem. Chem. Phys.* **2012**, *14*, 10896−10898.
(95) Zhang, B.; Zhu, Z.; Wang, X.; Liu, X.; Kapteijn, F. Water Adsorption in MOFs: Structures and Applications. *Adv. Funct. Mater.* **2024**, *34*, No. 2304788.
(96) Shih, S.-M.; Lin, L.-C. Water Adsorption in Metal−Organic Frameworks: Characteristics, Mechanisms, and Structure−Property Relationships. *J. Am. Chem. Soc.* **2025**, *147*, 34791−34803.
(97) Oladoja, N. A. A critical review of the applicability of Avrami fractional kinetic equation in adsorption-based water treatment studies. *Desalination and Water Treatment* **2016**, *57*, 15813−15825.
(98) Grigoriadis, C.; Duran, H.; Steinhart, M.; Kappl, M.; Floudas, G. Suppression of Phase Transitions in a Confined Rodlike Liquid Crystal. *ACS Nano* **2011**, *5*, 9208−9215.
(99) Komangadi, M. A.; Zhuoqing, L.; Smales, G. J.; Pauw, B. R.; Wuckert, E.; Raab, A.; Laschat, S.; Huber, P.; Schönhals, A. Confiment -suppressed phase transition and dynamic self-assembly of ionic super discs in ordered nanochannels: Implications for nanoscale applications. *ACS Appl. Nano Mater.* **2023**, *6*, 15673−15684.
(100) Alba-Simionesco, C.; Coasne, B.; Dosseh, G.; Dudziak, G.; Gubbins, K. E.; Radhakrihnan, R.; Sliwinska-Bartkowiak, M. Effects of confinement on freezing and melting. *J. Phys.: Condens. Matter* **2006**, *18*, R15−R68.
(101) Havriliak, S.; Negami, S. A complex plane analysis of α-dispersions in some polymer systems. *J. Polym. Sci., Part C: Polym. Symp.* **1966**, *14*, 99−117.
(102) Schönhals, A.; Kremer, F. Analysis of Dielectric Spectra. In *Broadband Dielectric Spectroscopy*; Kremer, F.; Schönhals, A., Eds.; Springer: Berlin, Heidelberg, 2003; pp 59−98.
(103) Meyer, W. V.; Neldel, H. Über die Beziehung zwischen der Energiekonstanten c und der Mengenkonstante in der Leitwerts-Temperaturformel bei oxydischen Halbleitern. *Z. Technol. Phys.* **1937**, *18*, 588.
(104) Dyre, J. C. A phenomenological model for the Meyer-Neldel rule. *Solid State Phys.* **1986**, *19*, 5655.
(105) Yelon, A.; Movaghar, B.; Branz, H. M. Origin and consequences of the compensation (Meyer-Neldel) law. *Phys. Rev. B* **1992**, *B46*, 12244.
(106) Thoms, E.; Napolitano, S. Enthalpy-entropy compensation in the slow Arrhenius process. *J. Chem. Phys.* **2023**, *159*, 161103.
(107) Schönhals, A.; Wolff, D.; Springer, J. Influence of the mesophase structure on the β-relaxation in comb-like polymethacrylates. *Macromolecules* **1995**, *28*, 6254−6257.
(108) Zorn, R.; Szymoniak, P.; Kolmangadi, M. A.; Malpass-Evans, R.; McKeown, N. B.; Jalavo, N. H.; Tyagi, M.; Böhning, M.; Schönhals, A. Microscopic Molecular Mobility of High-Performance Polymers of Intrinsic Microporosity revealed by Neutron Scattering − Bend Fluctuations and Signature of Methyl Group Rotation. *Soft Matter* **2024**, *20*, 5153−5164.
(109) Beiner, M. Huth Nanophase separation and hindered glass transition in side-chain polymers. *Nat. Mater.* **2003**, *2*, 595−599.
(110) Schönhals, A.; Kremer, F. Theory of dielectric relaxation. In *Broadband Dielectric Spectroscopy*; Kremer, F.; Schönhals, A., Eds.; Springer: Berlin, Heidelberg, 2003; pp 1−33.
(111) Dudziak, M.; Richerts, B.; Maaß, R.; Michalchuk, A.; Schönhals, A.; Szymoniak, P. Beyond conventional calorimetry: Unlocking thermal characterization with fast scanning techniques. *Thermochm. Acta* **2025**, *754*, No. 180177.
(112) Dyre, J. C.; Schrøder, T. B. Universality of ac conduction in disordered solids. *Rev. Mod. Phys.* **2000**, *72*, 873−892.
(113) Jonscher, A. K. The 'Universal' Dielectric Response. *Nature* **1977**, *267*, 673−679.
(114) Kremer, F.; Różański, S. A. The dielectric properties of semiconducting disordered materials. In *Broadband Dielectric Spectroscopy*; Kremer, F.; Schönhals, A., Eds.; Springer: Berlin, Heidelberg, 2003; pp 475−494.
(115) Vogel, H. Das Temperaturabhängigkeitsgesetz der Viskosität von Flüssigkeiten. *Phys. Z.* **1921**, *22*, 645−646.
(116) Fulcher, G. S. Analysis of Recent Measurements of the Viscosity of Glasses. *J. Am. Ceram. Soc.* **1925**, *8*, 339−355.
(117) Tammann, G.; Hesse, W. Die Abhängigkeit der Viskosität von der Temperatur bei unterkühlten Flüssigkeiten. *Z. Anorg. Allg. Chem.* **1926**, *156*, 245−257.
(118) Beilinson, Y.; Schiller, V.; Regentin, J.; Melillo, J. H.; Greenbaum, A.; Antropova, T.; Cerveny, S.; Vogel, M.; Feldmann, Y. The nature of the low-temperature crossover of water in hard confinement. *J. Phys. Chem. B* **2023**, *127*, 5128−5140.

https://doi.org/10.1021/acs.jpcc.6c02160
J. Phys. Chem. C XXXX, XXX, XXX−XXX